Stiffness analisys of the Tripteron parallel manipulator

1st Daniil Kirsanov
Innopolis University
Innopolis, Russia
d.kirsanov@innopolis.university

2nd Ilia Sevostianov
Innopolis University
Innopolis, Russia
i.sevostianov@innopolis.university

3rd Oleg Rodionov
Innopolis University
Innopolis, Russia
o.rodionov@innopolis.university

4th Mikhail Ostanin
Center for Technologies in Robotics and Mechatronics Components
Innopolis University
Innopolis, Russia
m.ostanin@innopolis.ru

***Abstract*—This article was devoted to the stiffness modeling of parallel robot Tripteron, which contains 3 separate legs directed along axes X, Y and Z. Two different techniques, Virtual joint modeling(VJM) and Matrix structural analysis(MSA) were applied in order to obtain the desired elastostatic model of the robot. Cartesian stiffness matrices were determined in a semi-analytical manner, corresponding deflections of the end-effector under external loads were represented in the form of deflection maps. Both approaches were analyzed and compared according to the computational cost and difference between results.**

***Index Terms*—Manipulator stiffness modeling, Parallel robot, Virtual joint modeling, Matrix structural analysis**

I. Introduction

Applications of modern parallel robots significantly depend on the tool accuracy. This is why more attention has recently been paid to the stiffness analysis of industrial manipulators which allows to evaluate the deflections of the end-effector(EE) under the applied loads. At the same time, much interest is directed to parallel structures, which have some advantages over serial robots, such as higher payload since this it has several chains and higher structural stiffness [1].

There are 3 modern techniques for stiffness modeling in literature, which differ in accuracy, complexity and computational expenses. The most precise is FEA(Finite element analysis) [2], [3], which considers the design as a set of simple elements with known stiffness matrices and combining them makes up the global stiffness matrix of the entire structure. The drawbacks of this method are high computational cost and necessity of using true links dimensions and shapes. The matrix structural analysis (MSA) [4], [5] uses the same idea, but elements of the structure are either discarded or significantly simplified in order to reduce th complexity. The last one is the simplest one, virtual joint method (VJM) [6], [7], which is build on assumption that all the stiffness are concentrated in elastic elements(virtual joints), and all other parts of the structure are rigid.

The work presented in this paper is supported by RFBR project 18-38-20186\8.

The tripteron is a 3-DOF translational parallel mechanism which consist of 3 serial kinematic legs and the EE platform. A similar design is Quadrupteron [8] - a parallel robot with 4 degrees of freedom. The robot's features are the isotropy, that is the ability to make forward movements in all 3 directions and the separability, i.e. each of the actuators is controlling one Cartesian degree of freedom, independently from the others. As a parallel robot, it has some advantages over serial manipulators, such as the positioning of its actuators on the base, which reduces the moving inertia and thus allows rapid movements. The challenging tasks, regarding to this type of robot are designing and constructing, assembling and the vulnerability of the leg Z compared to the rest, related to the weight of the entire structure and the plate.

The kinematics and dynamics of this robot have already been derived in [9]. This robot has no singularities within its workspace [10] and its dexterity is always optimal.

II. Kinematics

In order to analyse the stiffness properties of the tripteron robot we need to derive the forward and inverse kinematic equations for each serial chain. The kinemtic scheme of the robot is presented in the fig. 1.

A. Forward

In each serial chain of the robot, the axes of the passive joint are parallel to the direction of the prismatic joint of the leg and this joint controls one of the Cartesian coordinates of the EE. As you can see the global coordinate frame is located in the origin of the leg Z and coincide with the local coordinate frame that attached to the first joint of this leg. The local frames for the other legs are located in the same way as for the leg Z - x-axis coincides with the first link of the leg and

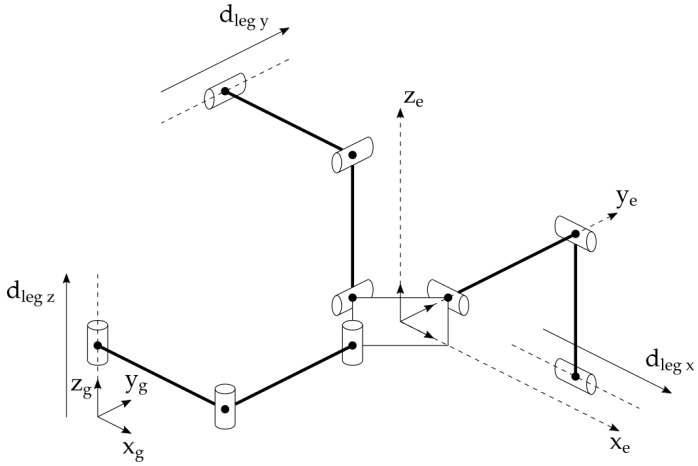

Fig. 1: Tripteron kinematics model

directed to the next joint and the z-axis lies along the axis of translation of the prismatic joint and directed in the way as shown on the kinematic scheme.

Since the robot under study consist of serial chains of the same structure the forward kinematics of a single chain i may be written as the product of the following homogenous matrices:

$$T = T_{base}T_z(d_i)R_z(q_{i,1})T_x(l_{i,1}) \\ R_z(q_{i,2})T_x(l_{i,2})R_z(q_{i,3})T_{tool} \quad (1)$$

where for the i-th serial chain of the robot d_i is the joint variable or displacement of the prismatic joint, $q_{i,j}$ is the joint variable of the j-th passive joint, $l_{i,j}$ is the length of the j-th link. T_{base} is the matrix that describes transform from the global coordinate frame to the local one of the single chain which of course are not the same for each leg and T_{tool} is the matrix that describes transform from the end of the single leg to the EE of the robot. Should be noted that due to the robot structure global and EE frame have the same orientation, thus, T_{tool} is the matrix that contain only rotation part which actually is the inverse of the rotation part of T_{base} matrix.

B. Inverse

The inverse kinematics of the whole robot can be written as

$$d_x = x_e, d_y = y_e, d_z = z_e \quad (2)$$

where x_e, y_e and z_e are the Cartesian coordinates of the EE.

The inverse kinematics of each separate leg in fact can be solved in the same way as the inverse kinematics of the two-link planar manipulator. The set of the following equations is the solution of the inverse kinematics for the separate leg in its local coordinate frame:

$$cos\ q_{i,2} = \frac{x^2 + y^2 - l_{i,1}^2 - l_{i,2}^2}{2l_{i,1}l_{i,2}} := D \quad (3)$$

$$sin\ q_{i,2} = \pm\sqrt{1 - D^2} \quad (4)$$

We can see that the equation (4) has two solution. where the positive solution corresponds to elbow-down configuration of the two links of the planar manipulator, and the negative one to elbow-up configuration. Due to the robot kinematics we use only positive solution of this equation in our study.

$$q_{i,2} = atan2(sin\ q_{i,2}, cos\ q_{i,2}) \quad (5)$$

$$q_{i,1} = atan2(y, x) - \\ - atan2\left(l_{i,2}sin\ q_{i,2},\ l_{i,1} + l_{i,2}cos\ q_{i,2}\right) \quad (6)$$

Since the EE frame has the same orientation as the global coordinate frame

$$q_{i,3} = -q_{i,1} - q_{i,2} \quad (7)$$

III. Stiffness of the links

We approximate links as cylindrical beams. In general case, the stiffness matrix K for a 3D beam element could be represented as following:

$$K = \begin{bmatrix} K_{11} & K_{12} \\ K_{21} & K_{22} \end{bmatrix} \quad (8)$$

where each sub-matrix has its own meaning: K_{11} describes force/torque reaction at the left-end point of the beam caused by the left-end deflection, K_{12} describes the force/torque reaction at the left-end point of the beam caused by the right-end deflection, K_{21} describes the force/torque reaction at the right-end of the beam point caused by the left-end deflection and K_{22} describes the force/torque reaction at the right-end point of the beam caused by the right-end deflection.

$$K_{11} = \begin{bmatrix} \frac{EA}{L} & 0 & 0 & 0 & 0 & 0 \\ 0 & \frac{12EI_z}{L^3} & 0 & 0 & 0 & \frac{6EI_z}{L^2} \\ 0 & 0 & \frac{12EI_y}{L^3} & 0 & -\frac{6EI_y}{L^2} & 0 \\ 0 & 0 & 0 & \frac{GI_\rho}{L} & 0 & 0 \\ 0 & 0 & -\frac{6EI_y}{L^2} & 0 & \frac{4EI_y}{L} & 0 \\ 0 & \frac{6EI_z}{L^2} & 0 & 0 & 0 & \frac{4EI_z}{L} \end{bmatrix}$$

$$K_{12} = \begin{bmatrix} -\frac{EA}{L} & 0 & 0 & 0 & 0 & 0 \\ 0 & -\frac{12EI_z}{L^3} & 0 & 0 & 0 & -\frac{6EI_z}{L^2} \\ 0 & 0 & -\frac{12EI_y}{L^3} & 0 & \frac{6EI_y}{L^2} & 0 \\ 0 & 0 & 0 & -\frac{GI_\rho}{L} & 0 & 0 \\ 0 & 0 & -\frac{6EI_y}{L^2} & 0 & \frac{2EI_y}{L} & 0 \\ 0 & \frac{6EI_z}{L^2} & 0 & 0 & 0 & \frac{2EI_z}{L} \end{bmatrix}$$

$$K_{21} = K_{12}^T$$

$$K_{22} = \begin{bmatrix} \frac{EA}{L} & 0 & 0 & 0 & 0 & 0 \\ 0 & \frac{12EI_z}{L^3} & 0 & 0 & 0 & -\frac{6EI_z}{L^2} \\ 0 & 0 & \frac{12EI_y}{L^3} & 0 & \frac{6EI_y}{L^2} & 0 \\ 0 & 0 & 0 & \frac{GI_\rho}{L} & 0 & 0 \\ 0 & 0 & \frac{6EI_y}{L^2} & 0 & \frac{4EI_y}{L} & 0 \\ 0 & -\frac{6EI_z}{L^2} & 0 & 0 & 0 & \frac{4EI_z}{L} \end{bmatrix}$$

and L is the beam length, I_y and I_z represent the principle moment of inertia, I_ρ represents the torsional moment of inertia, E and G are Young's and Coulomb's modules of the beam material (we assume that the robot consist of aluminum beams), respectively.

IV. Virtual Joint Modelling

The VJM model of the tripteron is presented in the figure 2. Since in this model we have additional component such as 1-DOF virtual springs after the active joints and the 6-DOF virtual springs after the rigid links we need to extend the forward kinematics equation (1) to the following form:

$$T = T_{base_i} T_z(d_i) T_z(\theta_{i,1}) R_z(q_{i,1}) T_x(l_{i,1}) T_{3D}(\theta_{i,2-7}) R_z(q_{i,2}) T_x(l_{i,2}) T_{3D}(\theta_{i,8-13}) R_z(q_{i,3}) T_{tool_i} \quad (9)$$

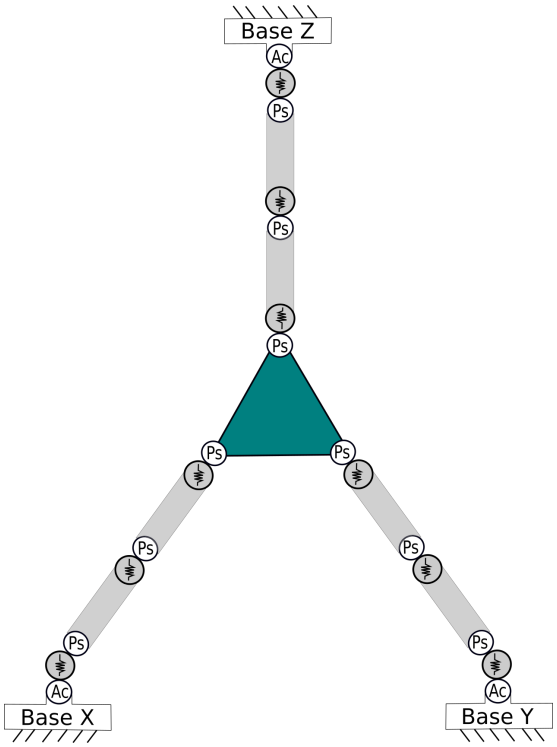

Fig. 2: VJM model

where $\theta_{i,j}$ is the variable of the j-th virtual joint in the i-th leg. The $T_{3D}(\theta_{i,j-(j+5)})$ is the 6-DOF virtual spring which can be consider as the next series of the transformations:

$$T_{3D}(\theta_{i,j-(j+5)}) = T_x(\theta_{i,j}) T_y(\theta_{i,j+1}) T_z(\theta_{i,j+2}) R_x(\theta_{i,j+3}) R_y(\theta_{i,j+4}) R_z(\theta_{i,j+5}) \quad (10)$$

For each chain we can find classical Cartesian stiffness matrix

$$K^0_{c,i} = \left(J_{\theta,i} K^{-1}_{\theta,i} J^T_{\theta,i} \right)^{-1} \quad (11)$$

where the J_θ is the jacobian with respect to the virtual joint variables calculated numerically and the K_θ is the aggregated spring stiffness matrix, which is the diagonal matrix consists of the stiffness parameters of the flexible part of the serial chain. In our case it is matrix 13×13 with the three main diagonal parts: scalar number which represents the stiffness of the active joint (in our case 10^6 H/m) and two stiffness matrices 6×6 represents the stiffness properties to the links. Since the virtual joint is located on the right-end of the link in out model we use K_{22}, because we're interested in force/torque reaction at right-end point of the beam caused by the right-end deflection.

We can use classical Cartesian stiffness matrix K^0_c in order to find Cartesian stiffness matrix of the single chain i:

$$K_{c,i} = K^0_{c,i} - K^0_{c,i} J_{q,i} K_{Cq,i} \quad (12)$$

where

$$K_{Cq,i} = \left(J^T_{q,i} \left(K^0_{C,i} \right)^{-1} J_{q,i} \right)^{-1} J^T_{q,i} \left(K^0_{C,i} \right)^{-1} \quad (13)$$

where the J_q is the Jacobian with respect to the passive joint variables calculated numerically.

For the parallel robot under study we can find Cartesian stiffness matrix K_c of the whole robot as the sum of the Cartesian stiffness matrices of the serial chains. Therefore,

$$K_c = \sum_{i=1}^{n} K_{ci} \quad (14)$$

In order to find the EE displacement Δt we can use the the Hook's law:

$$W = K_c \Delta t \quad (15)$$

where W is the wrench applied to the EE.

V. Matrix Structural Analysis

The MSA model of the tripteron is presented in figure 3. Each kinematic chain of the robot is described by the series of 8 nodes connected to the common rigid platform e and consists of rigid base at the node 1, active joint 1-2, two rigid links 2-3 and 8-e, three passive joints 3-4, 5-6 and 7-8, and two flexible links 4-5 and 6-7. The only part of the model that is not connected directly to the robot base corresponds to the EE that interacts with the environment by applying the force/torque to the external objects. That part produces the boundary condition which is also necessary for computation of the Cartesian stiffness matrix of the robot.

The node 1 is connected to the rigid base and described by the following constraint equation:

$$\begin{bmatrix} 0_{6\times6} & I_{6\times6} \end{bmatrix} \begin{bmatrix} W_1 \\ \Delta t_1 \end{bmatrix} = 0_{6\times1} \quad (16)$$

Flexible links 4-5 and 6-7 have constraints on deflection and loading could be described as:

$$\begin{bmatrix} -I_{6\times6} & 0_{6\times6} & K^{11}_{i,j} & K^{12}_{i,j} \\ 0_{6\times6} & -I_{6\times6} & K^{21}_{i,j} & K^{22}_{i,j} \end{bmatrix} \begin{bmatrix} W_i \\ W_j \\ \Delta t_i \\ \Delta t_j \end{bmatrix} = \begin{bmatrix} 0_{6\times1} \\ 0_{6\times1} \end{bmatrix} \quad (17)$$

where i and j are the node numbers.

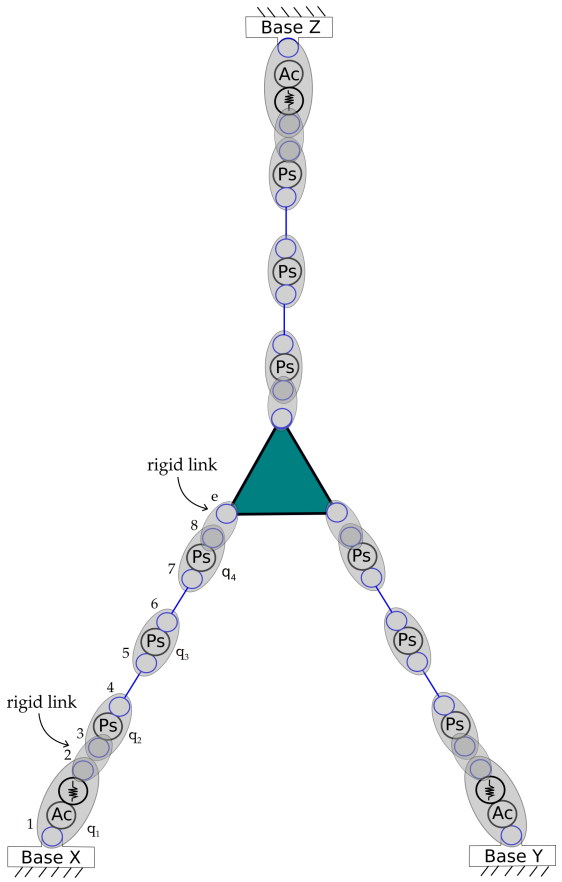

Fig. 3: MSA model

Rigid platform presented as a rigid link 8-e:

$$\begin{bmatrix} 0_{6\times6} & 0_{6\times6} & D_{8,e} & -I_{6\times6} \\ I_{6\times6} & D_{8,e}^T & 0_{6\times6} & 0_{6\times6} \end{bmatrix} \begin{bmatrix} W_8 \\ W_e \\ \Delta t_8 \\ \Delta t_e \end{bmatrix} = \begin{bmatrix} 0_{6\times1} \\ 0_{6\times1} \end{bmatrix} \tag{18}$$

where

$$D_{8,e} = \begin{bmatrix} I_{3\times3} & [d_{8,e}\times]^T \\ 0_{3\times3} & I_{3\times3} \end{bmatrix} \tag{19}$$

where $[d_{8,e}\times]$ is denotes the 3×3 skew-symmetric matrix derived from the vector $d_{8,e}$ which describes the link geometry and is directed from 8^{th} to e^{th} node. Since in our case we made an assumption that our rigid platform is just a point the vector $d_{8,e}$ actually has the magnitude of zero and, thus, $[d_{8,e}\times]^T = 0_{3\times3}$.

Therefore $D_{8,e} = I_{6\times6}$ and

$$\begin{bmatrix} 0_{6\times6} & 0_{6\times6} & I_{6\times6} & -I_{6\times6} \\ I_{6\times6} & I_{6\times6} & 0_{6\times6} & 0_{6\times6} \end{bmatrix} \begin{bmatrix} W_8 \\ W_e \\ \Delta t_8 \\ \Delta t_e \end{bmatrix} = \begin{bmatrix} 0_{6\times1} \\ 0_{6\times1} \end{bmatrix} \tag{20}$$

We can consider connection between the nodes 2 and 3 in the same way:

$$\begin{bmatrix} 0_{6\times6} & 0_{6\times6} & D_{2,3} & -I_{6\times6} \\ I_{6\times6} & D_{2,3}^T & 0_{6\times6} & 0_{6\times6} \end{bmatrix} \begin{bmatrix} W_2 \\ W_3 \\ \Delta t_2 \\ \Delta t_3 \end{bmatrix} = \begin{bmatrix} 0_{6\times1} \\ 0_{6\times1} \end{bmatrix} \tag{21}$$

and assuming that this link has the length equals 0:

$$D_{2,3} = I_{6\times6}$$

$$\begin{bmatrix} 0_{6\times6} & 0_{6\times6} & I_{6\times6} & -I_{6\times6} \\ I_{6\times6} & I_{6\times6} & 0_{6\times6} & 0_{6\times6} \end{bmatrix} \begin{bmatrix} W_2 \\ W_3 \\ \Delta t_2 \\ \Delta t_3 \end{bmatrix} = \begin{bmatrix} 0_{6\times1} \\ 0_{6\times1} \end{bmatrix} \tag{22}$$

Active elastic joint 1-2 is described by the following equation:

$$\begin{bmatrix} 0_{5\times6} & 0_{5\times6} & \lambda_{1,2}^r & -\lambda_{1,2}^r \\ I_{6\times6} & I_{6\times6} & 0_{6\times6} & 0_{6\times6} \\ \lambda_{1,2}^e & 0_{1\times6} & K_a\lambda_{1,2}^e & -K_a\lambda_{1,2}^e \end{bmatrix} \begin{bmatrix} W_1 \\ W_2 \\ \Delta t_1 \\ \Delta t_2 \end{bmatrix} = \begin{bmatrix} 0_{6\times1} \\ 0_{6\times1} \\ 0_{6\times1} \end{bmatrix} \tag{23}$$

where

$$\lambda_{1,2}^{e,x} = \begin{bmatrix} 1 & 0 & 0 & 0 & 0 & 0 \end{bmatrix} \tag{24}$$

$$\lambda_{1,2}^{e,y} = \begin{bmatrix} 0 & 1 & 0 & 0 & 0 & 0 \end{bmatrix} \tag{25}$$

$$\lambda_{1,2}^{e,z} = \begin{bmatrix} 0 & 0 & 1 & 0 & 0 & 0 \end{bmatrix} \tag{26}$$

$$\lambda_{1,2}^{r,x} = \begin{bmatrix} 0 & 1 & 0 & 0 & 0 & 0 \\ 0 & 0 & 1 & 0 & 0 & 0 \\ 0 & 0 & 0 & 1 & 0 & 0 \\ 0 & 0 & 0 & 0 & 1 & 0 \\ 0 & 0 & 0 & 0 & 0 & 1 \end{bmatrix} \tag{27}$$

$$\lambda_{1,2}^{r,y} = \begin{bmatrix} 1 & 0 & 0 & 0 & 0 & 0 \\ 0 & 0 & 1 & 0 & 0 & 0 \\ 0 & 0 & 0 & 1 & 0 & 0 \\ 0 & 0 & 0 & 0 & 1 & 0 \\ 0 & 0 & 0 & 0 & 0 & 1 \end{bmatrix} \tag{28}$$

$$\lambda_{1,2}^{r,z} = \begin{bmatrix} 1 & 0 & 0 & 0 & 0 & 0 \\ 0 & 1 & 0 & 0 & 0 & 0 \\ 0 & 0 & 0 & 1 & 0 & 0 \\ 0 & 0 & 0 & 0 & 1 & 0 \\ 0 & 0 & 0 & 0 & 0 & 1 \end{bmatrix} \tag{29}$$

The passive joints 3-4, 5-6 and 7-8:

$$\begin{bmatrix} 0_{5\times6} & 0_{5\times6} & \lambda_{i,j}^r & -\lambda_{i,j}^r \\ \lambda_{i,j}^r & \lambda_{i,j}^r & 0_{5\times6} & 0_{5\times6} \\ \lambda_{i,j}^p & 0_{1\times6} & 0_{1\times6} & 0_{1\times6} \\ 0_{1\times6} & \lambda_{i,j}^p & 0_{1\times6} & 0_{1\times6} \end{bmatrix} \begin{bmatrix} W_i \\ W_j \\ \Delta t_i \\ \Delta t_j \end{bmatrix} = \begin{bmatrix} 0_{6\times1} \\ 0_{6\times1} \\ 0_{6\times1} \\ 0_{6\times1} \end{bmatrix} \tag{30}$$

where

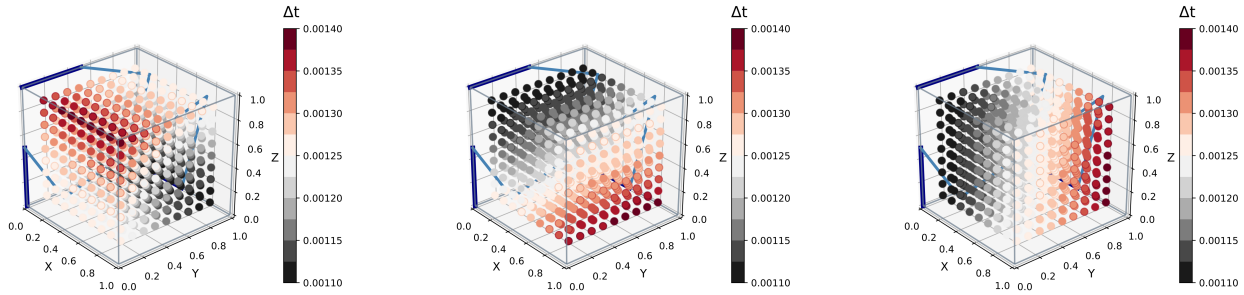

(a) Deflection 3D map for the applied wrench $W = [1000, 0, 0, 0, 0, 0]$

(b) Deflection 3D map for the applied wrench $W = [0, 1000, 0, 0, 0, 0]$

(c) Deflection 3D map for the applied wrench $W = [0, 0, 1000, 0, 0, 0]$

Fig. 4: Deflection 3D maps

$$\lambda_{3,4}^{p,x} = \lambda_{5,6}^{p,x} = \lambda_{7,8}^{p,x} = \begin{bmatrix} 0 & 0 & 0 & 1 & 0 & 0 \end{bmatrix} \tag{31}$$

$$\lambda_{3,4}^{p,y} = \lambda_{5,6}^{p,y} = \lambda_{7,8}^{p,y} = \begin{bmatrix} 0 & 0 & 0 & 0 & 1 & 0 \end{bmatrix} \tag{32}$$

$$\lambda_{3,4}^{p,z} = \lambda_{5,6}^{p,z} = \lambda_{7,8}^{p,z} = \begin{bmatrix} 0 & 0 & 0 & 0 & 0 & 1 \end{bmatrix} \tag{33}$$

$$\lambda_{3,4}^{r,x} = \lambda_{5,6}^{r,x} = \lambda_{7,8}^{r,x} = \begin{bmatrix} 1 & 0 & 0 & 0 & 0 & 0 \\ 0 & 1 & 0 & 0 & 0 & 0 \\ 0 & 0 & 1 & 0 & 0 & 0 \\ 0 & 0 & 0 & 0 & 1 & 0 \\ 0 & 0 & 0 & 0 & 0 & 1 \end{bmatrix} \tag{34}$$

$$\lambda_{3,4}^{r,y} = \lambda_{5,6}^{r,y} = \lambda_{7,8}^{r,y} = \begin{bmatrix} 1 & 0 & 0 & 0 & 0 & 0 \\ 0 & 1 & 0 & 0 & 0 & 0 \\ 0 & 0 & 1 & 0 & 0 & 0 \\ 0 & 0 & 0 & 1 & 0 & 0 \\ 0 & 0 & 0 & 0 & 0 & 1 \end{bmatrix} \tag{35}$$

$$\lambda_{3,4}^{r,z} = \lambda_{5,6}^{r,z} = \lambda_{7,8}^{r,z} = \begin{bmatrix} 1 & 0 & 0 & 0 & 0 & 0 \\ 0 & 1 & 0 & 0 & 0 & 0 \\ 0 & 0 & 1 & 0 & 0 & 0 \\ 0 & 0 & 0 & 1 & 0 & 0 \\ 0 & 0 & 0 & 0 & 1 & 0 \end{bmatrix} \tag{36}$$

The external loading denotes by the following equation:

$$\begin{bmatrix} -I_{6\times6} & 0_{6\times6} \end{bmatrix} \begin{bmatrix} W_e \\ \Delta t_e \end{bmatrix} = W_{ext} \tag{37}$$

Using all above-mentioned relationships (16)-(37) we can create aggregated equation (A term of the following equation can be found in appendix):

$$\begin{bmatrix} A_{102\times102} & B_{102\times6} \\ C_{6\times102} & D_{6\times6} \end{bmatrix} \begin{bmatrix} W_{ag54\times1} \\ \Delta t_{ag48\times1} \\ \Delta t_e \end{bmatrix} = \begin{bmatrix} 0_{102\times1} \\ W_{ext} \end{bmatrix} \tag{38}$$

and find the total stiffness matrix of the kinematic chain using the following formula:

$$K_c = D - CA^{-1}B \tag{39}$$

VI. Results

We implemented and applied both VJM and MSA approaches in order to obtain Cartesian stiffness matrix of the whole robot. After that we used equation (15) to find the deflection of the EE in different points of the robot workspace. We assumed that the latter is a cube with a side of 1 m. We also assumed that each link of our robot has the length 0.75 m and the diameter 0.15 m.

Figures 4a, 4b, 4c and 5 present scatter plots in 3D space where the X, Y, Z are the axis of the global coordinate frame and the color of the point represents the deflection of the EE in that point. The only difference between those figures is the value of the wrench that was applied to the robot EE. In the figures 4a, 4b, 4c applied only force with the magnitude of 1000 N in the position direction of the X, Y, Z axis, respectively. Fig. 5 shows the maximum deflections with 1000 N force applied in any direction.

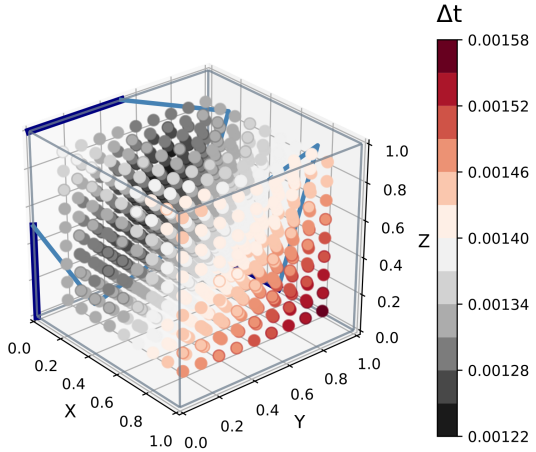

Fig. 5: Maximum deflections

According to deflection map analysis, we visually notice that if a force is applied along the j axis, then the deflection of EE depends only on the distance from the joint along the

j axis. For example, in plot 4b, the force is applied along the y axis, and the maximum deflection is along the line on the opposite edge of the workspace from joint along y. On the graph with the maximum possible deflections of the EE with the 1000 N force, it can be seen that the maximum deflection of the robot is at the point most remote from the robot axes along Y and Z, that confirms our statement above. In addition, deflection at points (1, 0, 0), (1,0,1) and (1,1,1) are equal, since these points are equally distant from 3 different axes, namely from 2 axes at a distance of 1 m, and from 3rd to $\sqrt{2}$ m distance.

VII. VJM and MSA Comparison

After we implemented VJM and MSA approaches for the parallel robot Tripteron, we decided to compare the total computation time and result deflection map. Total time is what we need to calculate the EE deflection in each point of the workspace. We run the program that calculates the deflection using the VJM method 100 times and calculated the average time that we need. The later is 1 minute and 37 seconds. We did the same for the MSA method and figure out that for it we need much less time which is 4.5 seconds. Thus for our particular implementation the MSA method is about 22 times faster than VJM. The difference between VJM and MSA result presented in figure 6. The high difference value power is 10^{-15}. That significant lower than deflections absolute values, it can be Python calculation error. So VJM and MSA results are equal.

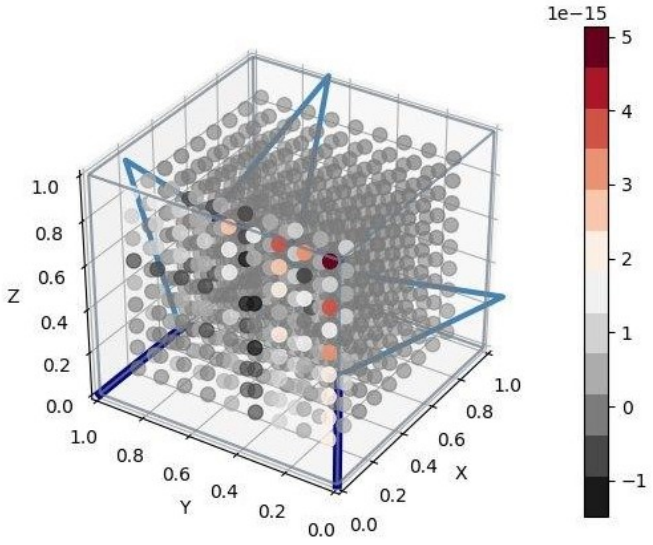

Fig. 6: Difference between VJM and MSA deflection map

Acknowledgment

VIII. Conclusion

Paper present the stiffens analysis of the parallel robot Tripteron. We implemented VJM and MSA approaches for stiffens modeling and find Cartesian stiffness matrix of the robot. Using Hook's law we have built deflection maps with 1000 N force applied along X,Y,Z direction and map with maximum deflections. We had note that for Tripteron robot if a force is applied along the j axis, then the deflection depends only on the distance from the joint along the j axis. Also in our work we compare the VJM and MSA approaches in execution time and difference between VJM and MSA deflection maps. We show that VJM and MSA results are equal for the parallel robot Tripteron.

References

[1] S. Staicu, "Spatial parallel robots," in *Dynamics of Parallel Robots*. Springer, 2019, pp. 191–243.

[2] H.-D. Do and K.-S. Park, "Analysis of effective vibration frequency of cable-driven parallel robot using mode tracking and quasi-static method," *Microsystem Technologies*, vol. 23, no. 7, pp. 2577–2585, 2017.

[3] S. Yan, S. Ong, and A. Nee, "Stiffness analysis of parallelogram-type parallel manipulators using a strain energy method," *Robotics and Computer-Integrated Manufacturing*, vol. 37, pp. 13–22, 2016.

[4] A. Klimchik, A. Pashkevich, and D. Chablat, "Fundamentals of manipulator stiffness modeling using matrix structural analysis," *Mechanism and Machine Theory*, vol. 133, pp. 365–394, 2019.

[5] D. Popov, V. Skvortsova, and A. Klimchik, "Stiffness modeling of 3rrr parallel spherical manipulator," 2019.

[6] A. Klimchik, "Enhanced stiffness modeling of serial and parallel manipulators for robotic-based processing of high performance materials," Ph.D. dissertation, 2011.

[7] H. Liu, T. Huang, D. G. Chetwynd, and A. Kecskeméthy, "Stiffness modeling of parallel mechanisms at limb and joint/link levels," *IEEE Transactions on Robotics*, vol. 33, no. 3, pp. 734–741, 2017.

[8] B. Danaei, A. Arian, M. T. Masouleh, and A. Kalhor, "Kinematic and dynamic modeling and base inertial parameters determination of the quadrupteron parallel manipulator," in *Computational Kinematics*. Springer, 2018, pp. 249–256.

[9] A. Arian, B. Danaei, and M. Tale Masouleh, "Kinematic and dynamic analyses of tripteron, an over-constrained 3-dof translational parallel manipulator, through newton-euler approach," *AUT Journal of Modeling and Simulation*, vol. 50, no. 1, pp. 61–70, 2018.

[10] Z. Anvari, P. Ataei, and M. T. Masouleh, "The collision-free workspace of the tripteron parallel robot based on a geometrical approach," in *Computational Kinematics*. Springer, 2018, pp. 357–364.